

Microporous SiO₂ and SiO₂/MO_x (M = Ti, Zr, Al) for Ceramic Membrane Applications: A Microstructural Study of the Sol-Stage and the Consolidated State

Code: E8

R.S.A. DE LANGE, K-N.P. KUMAR, J.H.A. HEKKINK, G.M.H. VAN DE VELDE,
K. KEIZER AND A.J. BURGGRAAF

University of Twente, Faculty of Chemical Technology, P.O.Box 217, 7500 AE Enschede, The Netherlands

W.H. DOKTER, H.F. VAN GARDEREN AND T.P.M. BEELEN

Technical University of Eindhoven, Faculty of Chemical Technology, P.O. Box 513, 5600 MB Eindhoven, The Netherlands

Abstract. Microporous SiO₂ and SiO₂/MO_x (M = Ti, Zr, Al; 10 mol% MO_x) materials for gas separation membrane applications have been prepared from polymeric sols. Characterization of these sols with SAXS showed that the mean fractal dimension of the SiO₂ sols is 1.3–1.4 with a radius of gyration of approximately 2.5 nm. The dried and calcined films are microporous and the pore size distribution was bimodal with maxima at diameters of 0.5 nm and 0.75 nm. For the SiO₂/TiO₂, SiO₂/ZrO₂ and SiO₂/Al₂O₃ systems, much milder reaction conditions proved to be necessary to obtain sols with comparable fractal dimensions due to the high reactivity of the Ti/Zr/Al-alkoxides. Microporous supported membranes with molecular sieve-like gas transport properties can be prepared from a relatively wide range of sol structures: from polymers too small to characterize with SAXS to structures with fractal dimensions: $1 < d_f < 2.04$.

Keywords: SiO₂, microporous, ceramic membrane, gas separation, microstructure

1. Introduction

In the inorganic membrane field, microporous materials ($r_p < 1$ nm [1]) are attracting more and more attention because of interesting, molecular sieve-like, gas separation properties [2, 3]. Sol-gel technology provides suitable methods for the preparation of microporous membranes, and successfully led to the development of microporous silica membranes [4, 5, 6, 7].

It is believed that for obtaining microporous materials, weakly branched polymeric sols have to be used [8]. The concept behind this is that interpenetration of weakly branched polymers leads to very fine pores. Tailoring of the sol morphology can be performed by controlling the hydrolysis and condensation of alkoxides in the sol-gel synthesis. If the conditions are chosen carefully, the sol morphology can be directed towards weakly branched polymeric systems or to particulate systems [9]. It is important to control the mechanism and the relative rates of the hydrolysis and condensation reactions [10]. For silica prepared from

TEOS (tetra-ethyl-ortho-silicate) under acid catalysed conditions, the hydrolysis is fast and the condensation is slow. Also both steps tend to form weakly branched structures under these conditions.

Since the reactivities of transition metal alkoxides are considerably higher than for silicon alkoxides [11], care has to be taken in the synthesis of binary materials to avoid homo-condensation. A commonly used strategy to avoid this is by a prehydrolysis process; the slowest reacting alkoxide is prehydrolyzed prior to the addition of the second, fast reacting, alkoxide [12].

In this paper we will focus on the relation between sol structure and structure of the consolidated dried and calcined (SiO₂, SiO₂/TiO₂, SiO₂/ZrO₂ and SiO₂/Al₂O₃ (10 mol% MO_x)) films. In the sol stage the structure is characterized with Small Angle X-ray Scattering (SAXS). Non-supported microporous membranes are characterized with N₂ adsorption. An important process parameter in the structural development is the drying condition during the sol-gel transition of the films. Some gas transport characteristics

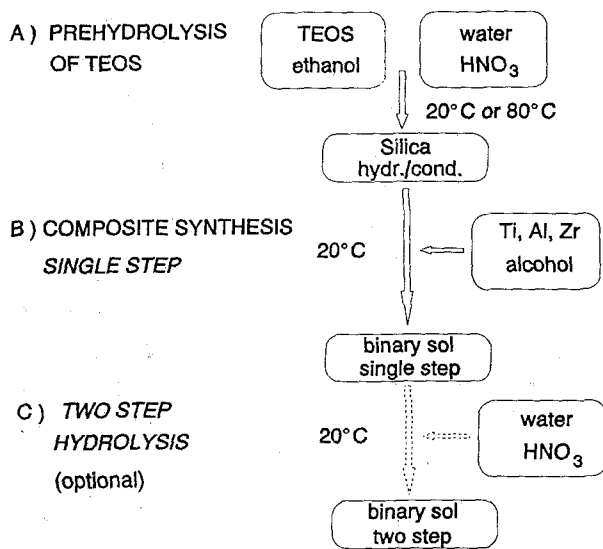


Fig. 1. Synthesis scheme of polymeric SiO_2/MO_x ($M = \text{Ti, Zr, Al}$) sols.

of supported microporous membranes are given to illustrate the range in which suitable structures can be formed. In the discussion we will elucidate the process parameters in the formation of microporous membranes from polymeric sols, and the problem of translating results obtained from non-supported membranes to supported membranes properties is addressed.

2. Experimental

Polymeric silica sols are prepared by acid catalysed (HNO_3 , Merck, p.a. grade) hydrolysis and condensation of TEOS (Merck p.a. grade) in ethanol (Merck, p.a. grade). A mixture of acid and water was carefully added, using a dropping funnel, to a mixture of ethanol and TEOS under vigorous stirring. The reaction mixture was then refluxed for 3 hours at 80°C under stirring. Molar ratios TEOS/ethanol/water/ HNO_3 are 1/3.8/6.4/0.085 (sample code StSiO_2).

Binary SiO_2 -based sols are prepared using TEOS, with $\text{Ti}(\text{O}^i\text{Pr})_4$ (Merck, p.a. grade) or $\text{Ti}(\text{O}^n\text{Bu})_4$ (Merck, p.a. grade), $\text{Zr}(\text{O}^n\text{Bu})_4 \cdot n\text{BuOH}$ (Alfa, p.a. grade) and $\text{Al}(\text{O}^s\text{Bu})_2$ -etac (Alfa, p.a. grade). The first step in the standard synthesis route (composite synthesis "Single step", Figure 1, samples "SiTi10", "SiZr10" and "SiAl10") is prehydrolysis of TEOS at 80°C for 3 hours ("SiTi10"), 20°C for 3 hours

("SiZr10") or 20°C for 1.5 hour ("SiAl10"). Molar ratios are Si/ethanol/water/ $\text{HNO}_3 = 1/3.8/1/0.085$ for "SiTi10" and "SiZr10", and Si/isopropanol/water/ $\text{HNO}_3 = 1/2.9/1.8/0.17$ for "SiAl10". The composite component in alcohol was added to the prehydrolysed TEOS at room temperature, and allowed to react for 2-3 hours. The composition and mol ratios, based on Si, of the alkoxide/alcohol mixtures are: Si/M/butanol = 1/0.11/2.5 for "SiTi10" and "SiZr10", and Si/Al propanol = 1/0.10/13.8 for "SiAl10".

For $\text{SiO}_2/\text{TiO}_2$ and $\text{SiO}_2/\text{ZrO}_2$, a second hydrolysis (so called *two step hydrolysis*, Figure 1, samples "SiTi10-2" and "SiZr10-2") was performed for some samples, 0.5 hour after the addition of the composite component. The ratio Si/ethanol/water/ HNO_3 after the first hydrolysis was 1/3.8/1.14/0.021 and 1/3.8/1/0.085 for samples "SiTi10-2" and "SiZr10-2" respectively. The composition of Ti/Zr-alkoxide/alcohol mixture in the composite step was Si/Ti/ethanol = 1/0.11/15.1 for "SiTi10-2" and Si/Zr/butanol = 1/0.11/2.5 for "SiZr10-2". After the second hydrolysis the total Si/ethanol/water/ HNO_3 ratio was 1/3.8/6.4/0.085 and 1/6.1/1.5/0.128 for "SiTi10-2" and "SiZr10-2" respectively.

A binary $\text{SiO}_2/\text{TiO}_2$ sol (sample "SiTi10X") was also prepared by mixing of separately prehydrolysed SiO_2 and TiO_2 sols. TEOS prehydrolysis was performed at 80°C as described before with Si/ethanol/water/ $\text{HNO}_3 = 1/3.8/4.6/0.085$. $\text{Ti}(\text{O}^i\text{Pr})_4$ prehydrolysis was performed at room temperature with Ti/ethanol/water/ $\text{HNO}_3 = 1/3.8/1/0.085$ (0.5 hour); water and acid were added in half the amount of ethanol to the ethanol/Ti(O^iPr)₄ solution. The binary sol was prepared by mixing the Ti-sol and the Si-sol, where the composition is adjusted to 10 mol% TiO_2 .

Small Angle X-ray scattering experiments on these sols were performed using synchrotron radiation (X-ray wave length $\lambda = 0.154 \text{ nm}$) at the Non-Crystalline Diffraction beamline 8.2 of the SERC Synchrotron Radiation Source (SRS), Daresbury (U.K.). The obtained spectra were corrected for background and parasitic scattering. The fractal dimension was calculated from the slope X of the linear part in the $\log(I)$ - $\log(Q)$ plot, where $D_f = -X$. The value of the radius of gyration was estimated from the cross-over point from the fractal region to the Guinier region with: $R_g \approx 1/Q_{\text{cross-over}}$.

Table 1. SAXS and N₂-adsorption results of SiO₂ and SiO₂/MO_x (M = Ti, Zr, Al) in comparison with supported membrane properties.

	Sol age (days)	SAXS		Non-supported#	Supported#		
		D_f (-)	R_g (nm)	Poros.* ϵ (%)	D_{eff} (nm)	$E_{act.}$ (H ₂) (kJ/mol)	α H ₂ /CH ₄ (-)
StSiO ₂	0	1.45	2.0	35-40	0.5/0.75	8-15	30-50
	10	1.65	3.0				
	20	1.75	3.5				
SiTi10 Bu, $r_w = 1$	4	-	-	42	0.5/0.75		
SiTi10 Bu, $r_w = 6.4$	4	1.9	5.1	7			
SiTi10 = 2 (Pr)	3	1.3	1.7	27	0.5/0.75	16	
SiTi10 = 2 (Bu)	3	1.3	1.7	28	0.5/0.75	8.4	
SiTi10X Pr	30	2.04	3.6	2			200
SiZr10	8	-	-	16	≈ 0.6		
SiZr10 = 2	6	1.43	0.84	2			
SiAl10	13	-	-	1		9.2	

- : No scattering

*: Porosity ϵ calculated using a skeletal density of 2.2 g/cm³, 2.36 g/cm³, 2.40 g/cm³ and 2.31 g/cm³ for amorphous silica, silica/titania, silica/zirconia and silica/alumina respectively.

#: Prepared from freshly prepared sols.

Non-supported microporous membranes were prepared by drying the freshly prepared sols in petri-dishes. Drying took place overnight under ambient conditions or during 3 hours in a climate chamber (Hereaus Vötsch VTRK 300) at 40°C/60% relative humidity and turbulent aerodynamic conditions (wind velocity 3.25 m/s). No coherent layers were obtained after drying, but the xerogels were cracked in flakes of 1 mm to 1–2 cm. The mean thickness of the non-supported membranes is 1–2 mm. Supported membranes were prepared by dipping mesoporous γ -alumina membranes (disc-shape, diameter 39 mm), with a high surface finish characterized by a mean roughness of 40 nm [13], in diluted, freshly prepared, polymeric sols (0.1 mol/l MO_x) for 4 seconds. The dried supported and non-supported samples were calcined in static air at 400°C for 3 hours, with a heating and cooling rate of 25°C per hour. The resulting materials were all X-ray amorphous [13].

Nitrogen adsorption measurements on calcined materials were performed with a Carlo Erba Sorptomatic

1900, extended with a turbo molecular pump system (Leybold PT50) and an extra pressure transducer (MKS Baratron type 122A) for the low pressure range (10⁻³ Torr to 10 Torr). All samples were degassed for 23 hours at 350°C at 10⁻⁶ Torr.

Pore size calculations were performed after the model of Harváth and Kawazoe [14], which was modified for Ar adsorption in cylindrical pores by Saito and Foley [15]. The proper physical constants have been substituted for N₂ adsorption [13]. For the calculation of the porosity, the liquid nitrogen density (0.808 g/cm³) is used for the density of nitrogen adsorbed in the micropores.

The used measurement area of the membranes for the permeation and separation experiments is 1.911 cm². Permeation experiments were performed using a dead-end configuration. Separation experiments were performed in a counter-current mode using argon as a sweep gas at the down-stream side. Typical gas flows for feed and sweep gas are 200 ml/min and 150 ml/min respectively. An extensive description of the

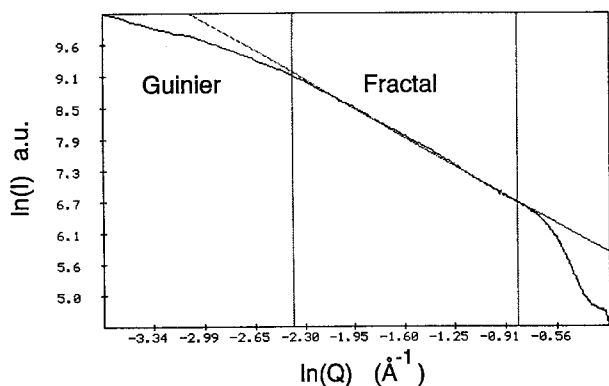


Fig. 2. SAXS spectrum of standard silica sol. $D_f = 1.47 \pm 0.07$, $R_g = 1.4 \pm 0.2$ nm.

used equipment for the permeation and separation experiments is given elsewhere [13, 16].

3. Results and Discussion

The results of this study of the sol structure and the microstructure of the consolidated materials have been summarized in Table 1. The (colourless and clear) silica sols consist of weakly branched fractal polymers, with a typical fractal dimension of 1.45 and radius of gyration of 1.4-2.2 nm directly after synthesis. Aging of the sols (in closed glass bottles) results in gelation after about 10 days, where $D_f = 1.65$ and $R_g = 3.0$ nm, followed by a further, less strong but gradual, increase of the fractal dimension to around 1.75 and radius of gyration of around 3.5 nm after 20 days. Further aging to 50 days does not change the gel structure significantly. The binary sols prepared according to the single step prehydrolysis process with low r_w in the prehydrolysis step (samples: “SiTi10Bu(toxide), $r_w = 1$ ”, “SiZr10” and “SiA110”) were also clear; however, with SAXS no scattering was detected. This implies that the structures may be too small to result in significant scattering with SAXS. Since a very low amount of water was used in the prehydrolysis (stoichiometric $r_w = 2$), the composite alkoxide can only condense with the hydrolysed silica, since it can be assumed that no free water is left. An increased water amount in the prehydrolysis step (“SiTi10Bu $r_w = 6.4$ ”) causes direct gelation of the sol during the addition of the Ti-alkoxide solution. Both the fractal dimension of this sol ($D_f = 1.9$) and the radius of gyration ($R_g = 5.1$ nm) are relatively high. The two-step processes lead to fractal structures with fractal dimensions of around 1.3 and radius of gy-

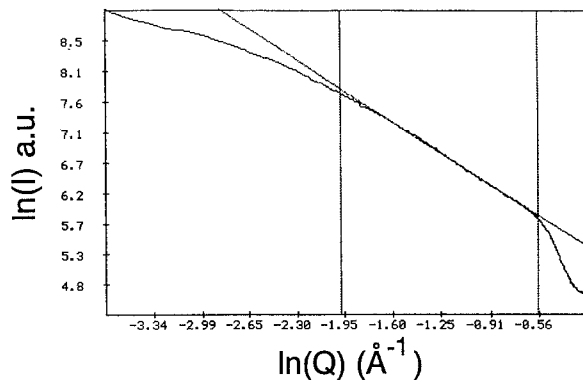


Fig. 3. SAXS spectrum of $\text{SiO}_2/\text{ZrO}_2$ sol “SiZr10-2”. $D_f = 1.43 \pm 0.07$, $R_g = 0.84 \pm 0.2$ nm.

ration of around 1.7 nm for “SiTi10-2” sols prepared with Ti-butoxide of Ti-isopropoxide. “SiZr10-2” has a slightly higher fractal dimension ($D_f = 1.43$) but lower radius of gyration ($R_g = 0.84$ nm). Sample “SiTi10X”, prepared by mixing of two prehydrolysed sols, has a relatively high fractal dimension (compared with silica sols of the same age) and a moderate radius of gyration.

Representative SAXS spectra for these polymeric sols are given in Figures 2 and 3. The SAXS spectrum of a standard silica sol is shown in Figure 2, and in Figure 3 the spectrum of silica- zirconia sol “SiZr10-2” is shown. A clear fractal region, which is less wide for the $\text{SiO}_2/\text{ZrO}_2$ sample, can be distinguished in both spectra. The slope is calculated using linear regression in the indicated regions.

The aggregation mechanism for the presented results, where a wide variation in fractal dimensions is shown, can not completely be explained by the rigid classical classification of aggregation models as for example diffusion limited cluster-cluster aggregation (DLCCA) or reaction limited cluster-cluster aggregation (RLCCA) [9]. The wide range in fractal dimensions, however, can be explained by differences in reactivity of the reacting species during the hydrolysis/condensation process, as is shown mathematically by Kallala [10].

The porosity (ε) and effective pore diameter (D_{eff}) of the (ambient) dried and subsequently calcined non-supported (bulk) materials, calculated from N_2 -adsorption isotherms, are given in Table 1. Some corresponding N_2 -isotherms are given in Figure 4, where it can be seen that the isotherm shape is typical for microporous materials [1]. The calculated pore size distributions (PSD) are given in Figure 5. The pore

Table 2. Influence of drying rate on porosity (ϵ) of non-supported silica.

SiO ₂ drying conditions	ϵ (%)	Drying time
Ambient	37	overnight
Climate Chamber	28	3 hours
Vacuum ($P \approx 2.4$ kPa)	31	overnight
Vacuum ($P \approx 0.1$ Pa)	0	overnight

size distribution, for both SiO₂ and the binary systems, looks to be bimodal with maxima at $D_{\text{effective}} = 0.5$ nm and 0.75 nm. The PSD's of the "SiTi10" samples are similar to silica. "SiZr10" and "SiTi10X", however, are less porous and the PSD's, which are less pronounced, show a somewhat larger effective pore diameter of around 0.6 nm. However, one should bear in mind that pore size calculations in the micropore region are still under discussion. Therefore, conclusions concerning absolute pore sizes are dangerous, although calibration with zeolites showed that the order of the calculated pore size is good [13].

As can be seen from Table 1, the relation between fractal dimension and porosity of the non-supported membranes is not straightforward. Very low porosities have been found for both sols with high fractal dimensions (samples "SiTi10Bu, $r_w = 6.4$ " and "SiTi10X"), moderate fractal dimension ("SiZr10-2") and sols with polymers too small to show scattering ("SiAl10"). Relatively high porosities have also been found for samples with low fractal dimensions ("SiTi10Bu, $r_w = 1$ " and "SiZr10") and moderate fractal dimensions ("StSiO₂" and SiTi10-2 Bu/Pr"). All these samples were dried overnight under ambient conditions. Further we have observed that increasing the water content in binary sol synthesis always leads to less porous materials, while the fractal dimensions increase! These observations show that a prediction of porosity of the consolidated materials based on fractal dimension alone is difficult.

This is also illustrated by drying experiments with standard silica sols in Table 2. It can be clearly seen that an increase of drying rate, either by introducing turbulent aerodynamic conditions and increased temperature in the climate chamber, or by imposing vacuum during the drying process, results in denser materials. Also it was observed that the maximum in

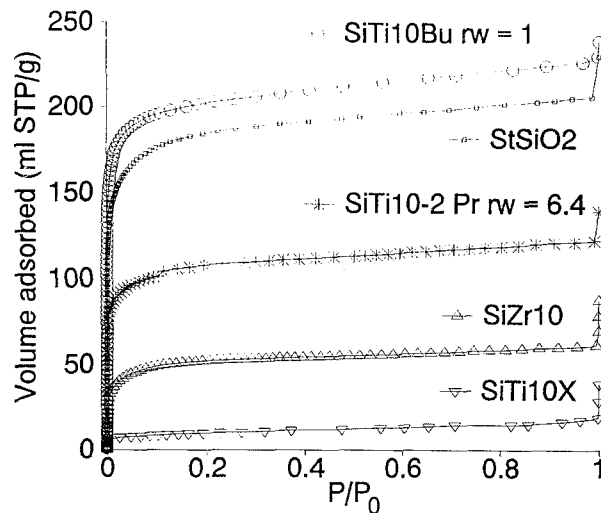


Fig. 4. N₂ absorption isotherm SiO₂ and SiO₂/MO_x (M = Ti, Zr).

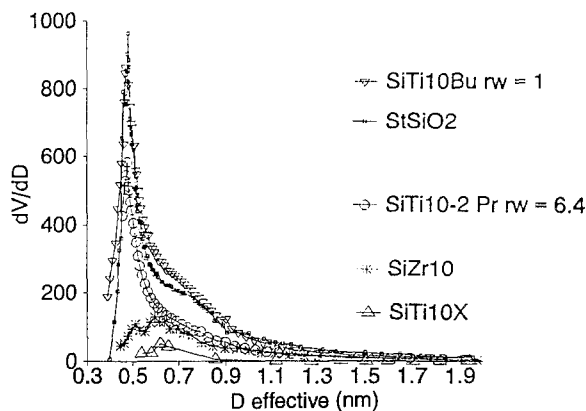


Fig. 5. Pore size distribution of SiO₂ and SiO₂/MO_x (M = Ti, Zr) according to the modified Horváth-Kawazoe model.

the pore size distribution at 0.75 is decreasing [13]. These results give the impression that interpenetration of the weakly branched polymers is hindered, resulting in higher porosities, if longer drying times are used. Proceeding condensation reactions, which may be regarded as an aging process, between the polymers during the drying process, will result in a stiffer structure. This allows the gel structure to withstand higher capillary forces during drying, resulting in a higher porosity. Analogous effects have been found for aging of water-glass derived silicas [17].

Obviously, the addition of more water for the binary sols results in internal condensation of the already formed structures. If no further growth takes place, the final radius of gyration can still be low. In spite of the

fact that interpenetration of these denser structures is hindered, denser consolidated structures are formed.

A selection of gas transport characteristics of supported membranes prepared from sols in a range of fractal dimensions is given in Table 1. Supported membrane thicknesses are in the order of 60–120 nm [13]. The most important characteristic of gas transport in microporous materials is activated transport, contrary to mesoporous materials where the permeation decreases as a function of temperature [3], and molecular sieve like separation factors (α). As can be seen, these transport properties are observed for both membranes corresponding with non-supported membranes with high porosities (“StSiO₂” and “SiTi10-2”) and non-supported membranes with low porosities (“SiTi10X” and “SiAl10”). The permeation rates, which are in the order of $15 \times 10^{-7} \text{ mol} \cdot \text{m}^{-2} \cdot \text{s}^{-1} \cdot \text{Pa}^{-1}$ for H₂ at 200°C for “StSiO₂”, however, are a factor 3–10 lower for the latter two membranes. This can not be explained by possible variations in membrane thicknesses alone. Although there is a distinct difference in the consolidation process for supported and non-supported membranes, these decreased permeation rates for the supported membranes look to be proportional with the porosities of non-supported materials.

These very interesting transport properties, show that the pore size of the supported membranes is very small, and in the order of the pore sizes found for the non-supported membranes. Based on the relatively high permeation rates of these membranes, and the order of the activation energy, which is relatively high for porous materials but low compared to dense glass, where activation energies of 38 kJ/mol have been reported for hydrogen [18], it can be concluded that transport takes place through micropores, and not through a dense layer!

The layer formation process for supported and non-supported membranes is significantly different on two points: i) The drying rates for supported systems are in the order of seconds contrary to hours for non-supported systems, which can result in denser systems as shown before and which was also reported by Frye and Brinker [19, 20]. ii) support constraints will hinder densification, as has been found for TiO₂-membranes by Kumar et al. [21].

These opposing effects on the structural formation of supported membranes make direct prediction of the supported membrane microstructure from non-

supported membrane characteristics difficult. Indirect methods, such as gas transport measurements, can give additional information.

4. Conclusions

It is shown that microporous, non-supported as well as supported, membranes can be made from inorganic polymeric sols with a relatively wide range of sol structures, from structures too small to characterize with SAXS to polymers with fractal dimensions $1 < D_f \leq 2.04$. The PSD of the non-supported materials was bimodal with maximum at an effective pore diameter of 0.5 nm and a weaker maximum at 0.7 nm. Based on the gas transport properties, it can be concluded that the pore size for supported membranes is of the same order. Drying conditions have shown to be very important in the structural development of the consolidated material, where higher drying rates result in denser structures. This implies that prediction of the final microstructure based on fractal geometry of the sols alone is difficult, and the chemistry and physics related with the drying process have to be taken into account. Consequently, translation of results from non-supported systems to supported systems can only be done with utmost care because of the difference in drying rates.

Acknowledgments

Shell Research, Amsterdam is gratefully acknowledged for general financial support. SAXS experiments were performed under terms of the SERC/NWO agreement. Special thanks to Dr. W. Bras of the SRS, Daresbury, for his kind help and valuable scientific discussions.

References

1. Sing, K.S.W., Everett, D.H., Haul, R.A.W., Moscou, L., Pierotti, R.A., Rouquérol, J., and Siemiewska, T., *Pure & Appl. Chem.*, **57** [4], 603 (1985).
2. Bhavé, R.R., *Inorganic membranes: Synthesis, Characteristics and Applications*, (Van Nostrand Reinhold, New York, 1991), Chapter 1.
3. Burggraaf, A.J., Keizer, K., de Lange, R.S.A., Vroon, Z.A.E.P., and Zaspalis, V.T., in: *Proceedings 9th Int. Zeolites Conf.*, Montreal, Canada, July 5–10, (1992), edited by Higgins, J.B., von Ballmoos, R. and Treacy, M.M.J., (Butterworth-Heinemann, Stoneham M.A., 1993), in press.

4. Uhlhorn, R.J.R., Keizer, K., and Burggraaf, A.J., *J. Membrane Sci.*, **66** [2 & 3], 271 (1992).
5. Kitao, S., Kameda, H., and Asaeda, M., *Membrane*, **15** [4], 222 (1990).
6. de Lange, R.S.A., Hekkink, J.H.A., Keizer, K., and Burggraaf, A.J., in *Better Ceramics through Chemistry V*, edited by Hampden-Smith, M.J., Klemperer, W.G., and Brinker, C.J., (Materials Research Society, Pittsburgh, 1992), 505.
7. Brinker, C.J., Ward, T.L., Sehgal, R., Raman, N.K., Hietala, S.L., Smith, D.M., Hua, D.-W., and Headley, T.J., *J. Membrane Sci.*, **77**, 165 (1993).
8. Brinker, C.J., Hurd, A.J., Schrunk, P.R., Frye, G.C., and Ashley, C.S. *J. Non-Cryst. Solids*, **147 & 148**, 424 (1992).
9. Brinker, C.J., and Scherer, G.W., *Sol-Gel Science. The Physics and Chemistry of Sol-Gel Processing* (Academic Press, San Diego, 1990).
10. Kallala, M., Jullien, R., and Cabane, B., *J. Phys. II France*, **2**, 7 (1992).
11. Livage, J., Henry, M., and Sanchez, C., *Prog. Solid St. Chem.*, **18**, 259 (1988).
12. Schraml-Marth, M., Walther, K.L., Wokaun, H., Handy, B.E., and Baiker, A., *J. Non-Cryst. Solids.*, **143**, 93 (1992).
13. de Lange, R.S.A., Ph-D Thesis, University of Twente, Enschede, Nov. (1993).
14. Horváth, G. and Kawazoe, K., *J. Chem. Eng. Japan*, **16** [6], 470 (1983).
15. Saito, A. and Foley, H.C., *AIChE Journal*, **37** [3], 429 (1991).
16. Uhlhorn, R.J.R., Keizer, K., and Burggraaf, A.J., *J. Membrane Sci.*, **66** [2 & 3], 259 (1992).
17. Dokter, W.H., Beelen, T.P.M., van Garderen, H.F., and van Santen, R.A., submitted for publication in *Proceedings IU-PAC Symp. COPS III*, Marseille, France, May 9-12, (1993), edited by Rouquérol, J., Rodriguez-Reinoso, F., Sing, K.S.W., and Unger, K.K., (Elsevier, Amsterdam, 1993).
18. Lee, R.W., *J. Chem. Phys.*, **38**, 448 (1963).
19. Frye, G.C., Ricco, A.J., Martin, S.J., and Brinker, C.J., in *Better Ceramics through Chemistry III*, edited by Brinker, C.J., Clark, D.E., and Ulrich, D.R. (Materials Research Society, Pittsburgh, 1988), 349.
20. Brinker, C.J., Frye, G.C., Hurd, A.J., and Ashley, C.S., *J. Non-Cryst. Solids*, **147 & 148**, 424 (1992).
21. Kumer, K-N.P., Keizer, K., Burggraaf, A.J., Okubo, T., and Nagamoto, H., *J. Mater. Chem.*, (1993), in press.